

# Costless-Function Model Predictive Current Control of Seven-Phase PMSM to Improve Dynamic Performance and Suppress Harmonics of Marine Electric Propulsion System

Xin Li, Wei Xie and Xiaoyan Xu

*Department of Electrical Engineering, Shanghai Maritime University, Shanghai 201306, China*

**Abstract:** In order to improve the dynamic performance and suppress current harmonic for seven-phase PMSM (permanent magnet synchronous motor), this paper proposed an MPCC (mode predict current control) scheme based on SVPWM (space vector pulse width modulation) technique. By this scheme, the 14 virtual voltage vectors are first calculated based on the principle: the voltage vector synthesized in the 3rd harmonic subspace and the 5th harmonic subspace should be zero, in each sampling period, the optimal voltage vector is directly selected from the 14 virtual voltage vectors to achieve the best output current performance of seven-phase PMSM. In addition, no cost function related calculations are required in the MPCC scheme, reducing the calculation time and improving the dynamic response of the system. The simulation model of the seven-phase PMSM vector control system is established by using the Simulink tool of MATLAB, and the effectiveness of the scheme will be presented.

**Key words:** Optimal voltage vector, seven-phase PMSM, MPCC, SVPWM, harmonic suppress.

## 1. Introduction

With the development of technology, traditional three-phase machines are widely used in various fields. In the naval industry, conventional three-phase machines are predominantly used. Recently, the use of electric machines with more than three phases (such as seven-phase) has considerably increased, notably for high power applications such as ship propulsion [1]. Seven-phase motor has the advantages of high power density, high torque-to-inertia ratio, and high efficiency, but also has the advantages of low torque ripple and high reliability [2].

Multiphase machines are fed by multiphase VSI (voltage-source-inverter), modulation and control schemes have been developed to drive a multiphase VSI, such as SVPWM (space vector pulse width

modulation) [3], DTC (direct torque control) [4, 5], FOC (field-oriented control) [6] and MPC (model-predictive controls) [7, 8]. MPCs are separated into two classes, direct predictive control (DPC) and dead-beat control noted as PPC (PWM predictive control) [2], PPC has been used in current control for inverters (MPCC (mode predict current control)), as well as for PMSM (permanent magnet synchronous motor) [9], where the duty cycles are calculated by using classical space vector PWM (SVPWM). MPCC has been considered as one of the most effective and simplest current control schemes for multiphase VSIs due to its simple and intuitive concept, fast dynamic response, its control flexibility [10], and it uses optimality framework with possibility for incorporation of various nonlinearities and constraints of practical nature [11].

However, large amounts of harmonic currents are generated by the multiphase power systems when they are fed by a multiphase PWM inverter and lead to the

---

**Corresponding author:** Xiaoyan Xu, Ph.D., professor, research fields: ship power parameter detection and power quality control.

decrease of the control performance. To solve this problem, domestic and foreign experts and scholars have conducted a lot of research. In Ref. [12], a strategy based on hysteresis MPC control and multi-step prediction is proposed to suppress harmonic current. Virtual voltage vectors are adopted to extend the control set of FCS-MPC in Refs. [13, 14], and also improved the performance of the system. In the above literature, there is a common feature: in the MPCC control strategy, the selection of the optimal voltage vector is determined by the loss function. The cost function undoubtedly increases the computing time of the system. In this paper, an FCS-MPC control strategy of seven-phase PMSM based on SVPWM is proposed. In the control strategy, the selection of the optimal voltage vector does not depend on the loss function, and the harmonic is suppressed by the combination of five basic voltage vectors. The dynamic response speed of the motor is improved.

In the next parts, the seven-phase PMSM model, the synthesis of virtual voltage vectors and the system simulation experiments will be elaborated. The system simulation experiments are implemented based on the MATLAB Simulink module.

## 2. Mathematical Model Description

This part describes the ideal mathematical model of seven-phase PMSM in the natural coordinate system and  $\alpha$ - $\beta$  coordinate system. Steady-state simulation is run to verify the rationality of the modeling.

### 2.1 Mathematical Model in the Natural Coordinate System

The phase voltage and the stator flux linkage equations in stator frame are shown as follows:

$$\mathbf{u}_s = \mathbf{R}_s \mathbf{i}_s + \frac{d}{dt} \boldsymbol{\psi}_s \quad (1)$$

$$\boldsymbol{\psi}_s = \mathbf{L}_s \mathbf{i}_s + \boldsymbol{\psi}_m \quad (2)$$

where  $\mathbf{u}_s = [u_A \ u_B \ u_C \ u_D \ u_E \ u_F \ u_G]^T$  and  $\mathbf{i}_s = [i_A \ i_B \ i_C \ i_D \ i_E \ i_F \ i_G]^T$  are the stator phase

voltage and current vectors respectively;  $\mathbf{R}_s = \text{dig}[R, R, R, R, R, R, R]$ ,  $R$  is the stator resistance of each phase;  $\mathbf{L}_s$  is the inductance matrix of the stator;  $\boldsymbol{\psi}_s$  is the stator flux matrix;  $\boldsymbol{\psi}_m$  is the permanent magnet flux vector, it can be expressed as:

$$\boldsymbol{\psi}_m = \psi \begin{bmatrix} \cos \theta \\ \cos(\theta - \alpha) \\ \cos(\theta - 2\alpha) \\ \cos(\theta - 3\alpha) \\ \cos(\theta - 4\alpha) \\ \cos(\theta - 5\alpha) \\ \cos(\theta - 6\alpha) \end{bmatrix} \quad (3)$$

where  $\psi$  is the flux linkage amplitude of permanent magnet,  $\theta$  is the rotor position angle, with electricity angle indication,  $\alpha$  is the angle between adjacent two-phase winding axes,  $\alpha = 2\pi/7$ .

The torque equation is:

$$T_e = \frac{1}{2} p_n \frac{\partial}{\partial \theta} (\mathbf{i}_s^T \cdot \boldsymbol{\psi}_m) \quad (4)$$

where  $p_n$  is the polar logarithm of motor.

### 2.2 Mathematical Model in $\alpha$ - $\beta$ Coordinate System

By using VSD (vector space decoupling), the seven-phase PMSM mathematical model in the natural coordinate system can be transformed into the  $\alpha$ - $\beta$  coordinate system. This model will be used in Section 3 of the MPCC control strategy.

The voltage and flux in  $\alpha$ - $\beta$  coordinate system can be obtained as in Eq. (5):

$$\mathbf{u}_{\alpha\beta} = \mathbf{R}_{\alpha\beta} \mathbf{i}_{\alpha\beta} + \mathbf{L}_{\alpha\beta} \frac{d}{dt} \mathbf{i}_{\alpha\beta} + \boldsymbol{\Phi}(\theta) \quad (5)$$

where  $\mathbf{u}_{\alpha\beta}$  and  $\mathbf{i}_{\alpha\beta}$  are the stator phase voltage and current vectors respectively under  $\alpha$ - $\beta$  coordinate system, including  $\alpha$ - $\beta$  space components, 3rd space component, 5th space component and zero-order space component [15].  $\mathbf{R}_{\alpha\beta} = \mathbf{T}_{\alpha\beta} \mathbf{R}_s \mathbf{T}_{\alpha\beta}^{-1}$ , is the  $\alpha$ - $\beta$  stator resistance matrix.  $\mathbf{L}_{\alpha\beta} = \mathbf{T}_{\alpha\beta} \mathbf{L}_s \mathbf{T}_{\alpha\beta}^{-1}$ , is the  $\alpha$ - $\beta$  inductance matrix of the stator.  $\boldsymbol{\Phi}(\theta) = \mathbf{T}_{\alpha\beta} \frac{d}{dt} \boldsymbol{\psi}_m$  is the component of the magnetic chain of permanent magnets on  $\alpha$ - $\beta$  space.

According to the matrix transformation of Clark, the transformation matrix from the natural coordinate system to  $\alpha$ - $\beta$  coordinate system is obtained:

$$T_{\alpha\beta} = \sqrt{\frac{2}{7}} \quad (6)$$

$$\begin{bmatrix} 1 & \cos(\alpha) & \cos(2\alpha) & \cos(3\alpha) & \cos(4\alpha) & \cos(5\alpha) & \cos(6\alpha) \\ 0 & \sin(\alpha) & \sin(2\alpha) & \sin(3\alpha) & \sin(4\alpha) & \sin(5\alpha) & \sin(6\alpha) \\ 1 & \cos(3\alpha) & \cos(6\alpha) & \cos(9\alpha) & \cos(12\alpha) & \cos(15\alpha) & \cos(18\alpha) \\ 0 & \sin(3\alpha) & \sin(6\alpha) & \sin(9\alpha) & \sin(12\alpha) & \sin(15\alpha) & \sin(18\alpha) \\ 1 & \cos(5\alpha) & \cos(10\alpha) & \cos(15\alpha) & \cos(20\alpha) & \cos(25\alpha) & \cos(30\alpha) \\ 0 & \sin(5\alpha) & \sin(10\alpha) & \sin(15\alpha) & \sin(20\alpha) & \sin(25\alpha) & \sin(30\alpha) \\ 1 & 1 & 1 & 1 & 1 & 1 & 1 \end{bmatrix}$$

### 2.3 Seven-Phase PMSM Model Simulation Results

By applying a standard sinusoidal AC current with a  $2\pi/7$  difference to a seven-phase PMSM, the motor output can be obtained (including stator current (A), rotor speed (rad/s), electromagnetic torque (N·m)), shown in Fig. 1.

As can be seen from Fig. 1, when the ideal power supply is input, in the steady state, the stator current is also ideal sinusoidal and  $2\pi/7$  from each other, and the speed is stable at the given value, and at 0.3 s, due to the sudden addition of load to 200 N·m, the electromagnetic torque reaches steady state after rapid fluctuations and is equal to the load torque. The basic performance requirements of the motor are met, and the model established is of practical significance.

## 3. Voltage Space and Motor MPCC

### 3.1 Voltage Space of Seven-Phase VSI

Seven-phase PMSM was fed by a two-level seven-phase VSI. The switch state of each bridge arm is defined as a switch value  $S_i$  ( $i = A, B, C, D, E, F, G$ ), when  $S_i = 1$ , it means that the upper switch of this bridge arm is closed and the lower switch is open, and when  $S_i = 0$ , the switch state is the opposite of the above. A total of  $2^7 = 128$  different switching states can be obtained by combining the switches of the seven bridge arms.

A seven-phase VSI can be described in three orthogonal planes, which are designed as  $\alpha$ - $\beta$ ,  $x_1$ - $y_1$

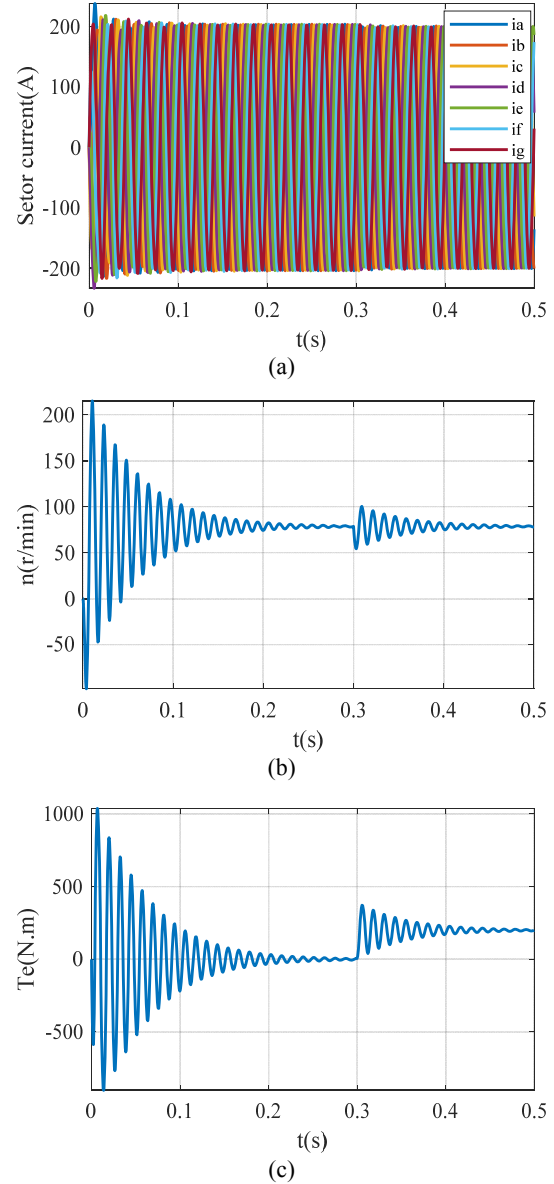


**Fig. 1** Motor output components at ideal power input with no load torque: (a) stator current, (b) rotor speed, (c) electromagnetic torque.

and  $x_2$ - $y_2$ , using Clarke's decomposition matrix for seven-phase systems. The voltage space in each plane can be defined as:

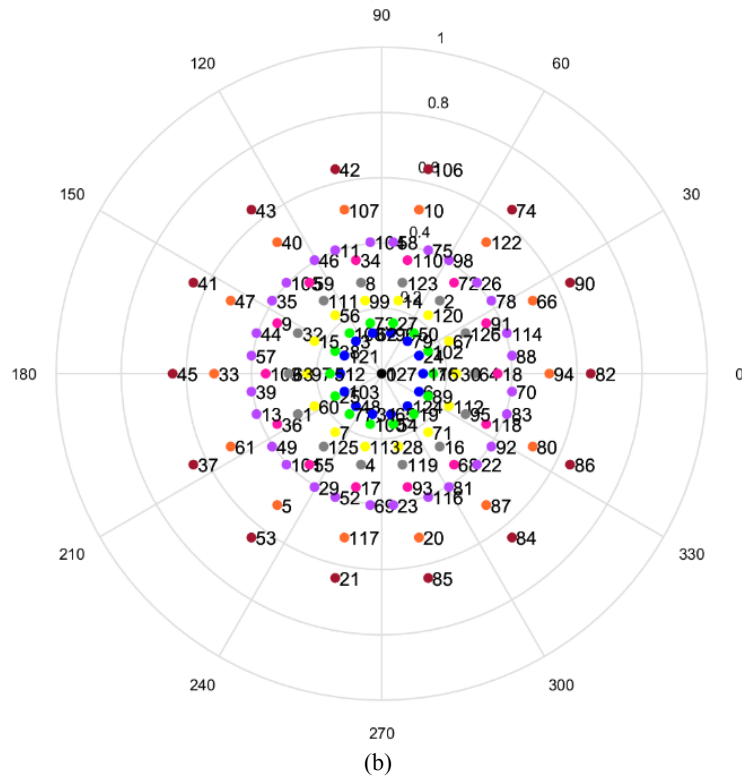
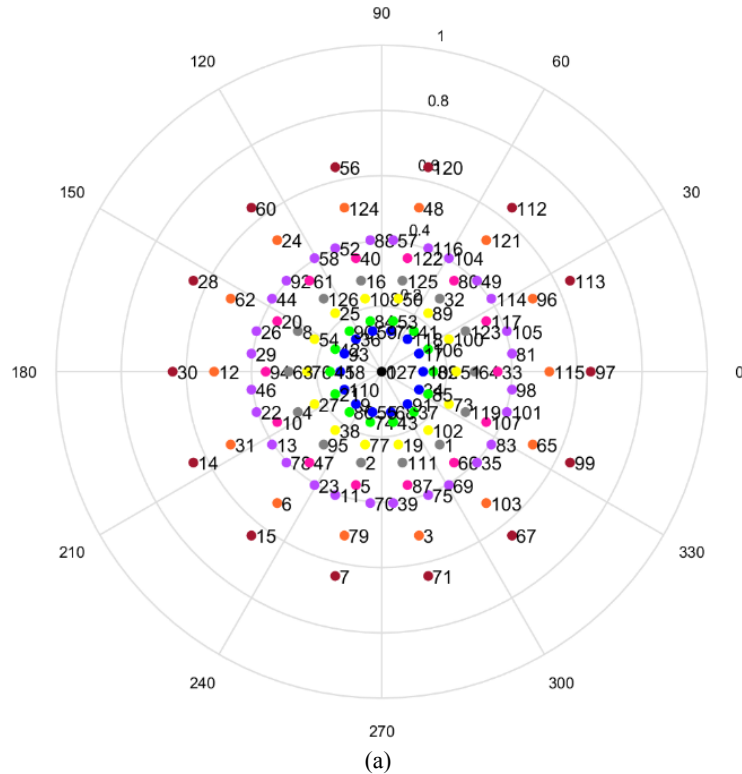
$$\begin{cases} V_{\alpha\beta} = \frac{2}{7}V_{dc}(S_a + \alpha S_b + \alpha^2 S_c + \alpha^3 S_d + \alpha^4 S_e + \alpha^5 S_f + \alpha^6 S_g) \\ V_{x_1y_1} = \frac{2}{7}V_{dc}(S_a + \alpha^3 S_b + \alpha^6 S_c + \alpha^2 S_d + \alpha^5 S_e + \alpha S_f + \alpha^4 S_g) \\ V_{x_2y_2} = \frac{2}{7}V_{dc}(S_a + \alpha^5 S_b + \alpha^3 S_c + \alpha S_d + \alpha^6 S_e + \alpha^4 S_f + \alpha^2 S_g) \end{cases} \quad (7)$$

where  $V_{dc}$  is the VSI DC side voltage,  $\alpha = 2\pi/7$ .

Assuming  $V_{dc} = 1$  V, the 128 switching states are brought into each of the three spaces in Eq. (7) to obtain the voltage space vector as shown in Fig. 2.

All subspaces can be divided into 9 groups

according to the magnitude of the voltage vectors, and the voltage vectors in each group have the same magnitude but different vector angles.  $\alpha$ - $\beta$  subspace voltage vectors are shown in Table 1.



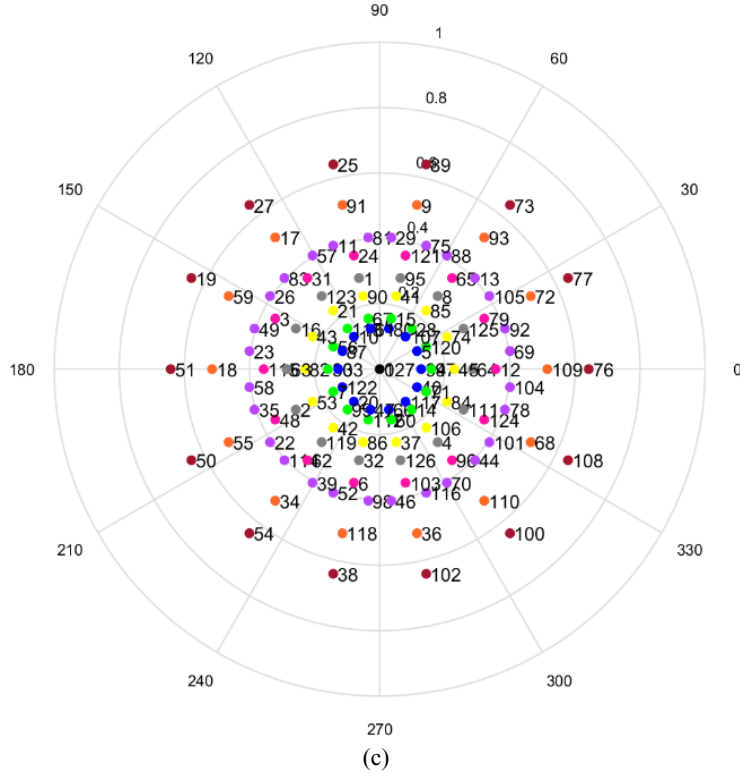


Fig. 2 Voltage vector space: (a)  $\alpha$ - $\beta$  subspace, (b)  $x_1$ - $y_1$  subspace, (c)  $x_2$ - $y_2$  subspace.

Table 1  $\alpha$ - $\beta$  subspace voltage vectors.

Group	Voltage vectors	$ V_{\alpha\beta} $
1	127,0	0
2	109,17,118,72,59,36,93,18,110,9,55,68,91,34	$0.1271V_{dc}$
3	82,106,41,53,84,90,42,45,21,86,74,43,37,85	$0.1586V_{dc}$
4	51,100,89,10,108,25,54,76,27,38,77,19,102,73	$0.2291V_{dc}$
5	64,123,32,125,16,4,8,63,126,95,2,111,1,119	$0.2857V_{dc}$
6	33,117,80,122,40,61,20,94,10,47,5,87,66,107	$0.3563V_{dc}$
7	81,105,49,114,104,57,116,88,52,58,92,44,26,29,46,22,13,78,23,11,70,39,75,69,35,83,101,98	$0.404V_{dc}$
8	115,96,48,121,24,62,124,12,31,6,79,3,103,65	$0.5148V_{dc}$
9	97,113,112,120,56,60,28,30,14,15,7,71,67,99	$0.624V_{dc}$

As introduced in the introduction, with the increase of the number of motor phases, the control methods will become more and more, so that the control algorithm will become more flexible. The same is true of multiphase inverters. For seven-phase VSI, the control algorithm should be considered under three

planes named as  $(\alpha$ - $\beta)$ ,  $(x_1$ - $y_1)$ , and  $(x_2$ - $y_2)$ ; seven-phase VSI needs one more plane compared with five-phase VSI or six-phase VSI [16]. In order to restrain the harmonics in the phase current, the basic principle of the seven-phase inverter control is that under the premise of ensuring the maximum amplitude of the  $\alpha$ - $\beta$  subspace synthetic voltage vector, the amplitude of the synthesized voltage vector in  $x_1$ - $y_1$  subspace and  $x_2$ - $y_2$  subspace is zero.

### 3.2 Prediction Model of Seven-Phase PMSM

Eq. (5) gives the voltage equation of seven-phase PMSM in the coordinate system. Taking the current as the state variable, it is rewritten as follows.

$$\frac{d}{dt} \mathbf{i}_{\alpha\beta} = \mathbf{A} \mathbf{i}_{\alpha\beta} + \mathbf{B} \mathbf{u}_{\alpha\beta} + \mathbf{C} \quad (8)$$

where

$$\mathbf{A} = -(\mathbf{L}_{\alpha\beta})^{-1} \mathbf{R}_{\alpha\beta}, \mathbf{B} = (\mathbf{L}_{\alpha\beta})^{-1}, \mathbf{C} = -(\mathbf{L}_{\alpha\beta})^{-1} \boldsymbol{\Phi}(\theta)$$

In a very small sampling time  $T_s$ , Eq. (8) is linearized according to the Forward Euler method.

$$\mathbf{i}_{\alpha\beta}(k+1) = \mathbf{G} \mathbf{i}_{\alpha\beta}(k) + \mathbf{H} \mathbf{u}_{\alpha\beta}(k) + \mathbf{M}(k) \quad (9)$$

where  $\mathbf{G} = (1 + \mathbf{A})T_s, \mathbf{H} = \mathbf{B}T_s, \mathbf{M} = \mathbf{C}T_s$

In each sampling period, the model prediction current control needs to calculate the voltage vector required in 3 spaces for use in judging the sectors, and the above equation is transformed and simplified to obtain the prediction equation for the voltage vector required in each sampling period in three spaces as follows:

$$\mathbf{u}_{\alpha\beta}^*(k) = \mathbf{H}^{-1}(\mathbf{i}_{\alpha\beta}^*(k+1) - \mathbf{G}\mathbf{i}_{\alpha\beta}(k) - \mathbf{M}(k)) \quad (10)$$

During the hardware implementation, the computational speed of the microcontroller is not infinite, and a large number of calculations for the model predictive control cause a delay in the output of the optimal voltage vector. To solve this problem, the two-step prediction method is usually applied to the model predictive control link. By advancing the prediction Eq. (10) by one sampling period, the value of the predicted current at the moment of  $(k+2)$  can be obtained.

$$\mathbf{u}_{\alpha\beta}^*(k+1) = \mathbf{H}^{-1}(\mathbf{i}_{\alpha\beta}^*(k+2) - \mathbf{G}\mathbf{i}_{\alpha\beta}(k+1) - \mathbf{M}(k+1)) \quad (11)$$

#### 4. Costless-Function MPCC Strategy

In order to suppress the 3rd and 5th harmonics generated by the VSI, 14 virtual voltage vectors synthesized from the fundamental voltage vectors will

be used as the optimal voltage vectors according to the basic principle of optimal vector synthesis. First, the actual voltage vector at the moment  $k+1$  is predicted according to the prediction model. Next, the virtual voltage vector closest to the current predicted voltage vector is selected as the optimal voltage vector at the moment  $k+1$  according to the closest distance principle and is applied to the pulse generator to generate the voltage signal. The MPCC scheme block diagram is shown in Fig. 3.

##### 4.1 Synthesis of Virtual Voltage Vectors

The virtual voltage vector is synthesized from the basic voltage vector, and the quality of the synthesized virtual voltage vector varies with the selection of different basic voltage aptitude.

According to the literature [17], the outermost voltage vector (Group 9) of Fig. 2a is selected as the basic voltage vector for synthesizing the virtual voltage vector in this paper. Group 9 has a high magnitude, which can improve the voltage utilization on the DC side of the VSI, and Group 9 acts on the VSI, the CMC (common mode current) between the neutral point on the DC side of the VSI and the neutral point of the motor is small, compared to other groups. The virtual voltage vector in the  $\alpha\text{-}\beta$  coordinate system is shown in Fig. 4.

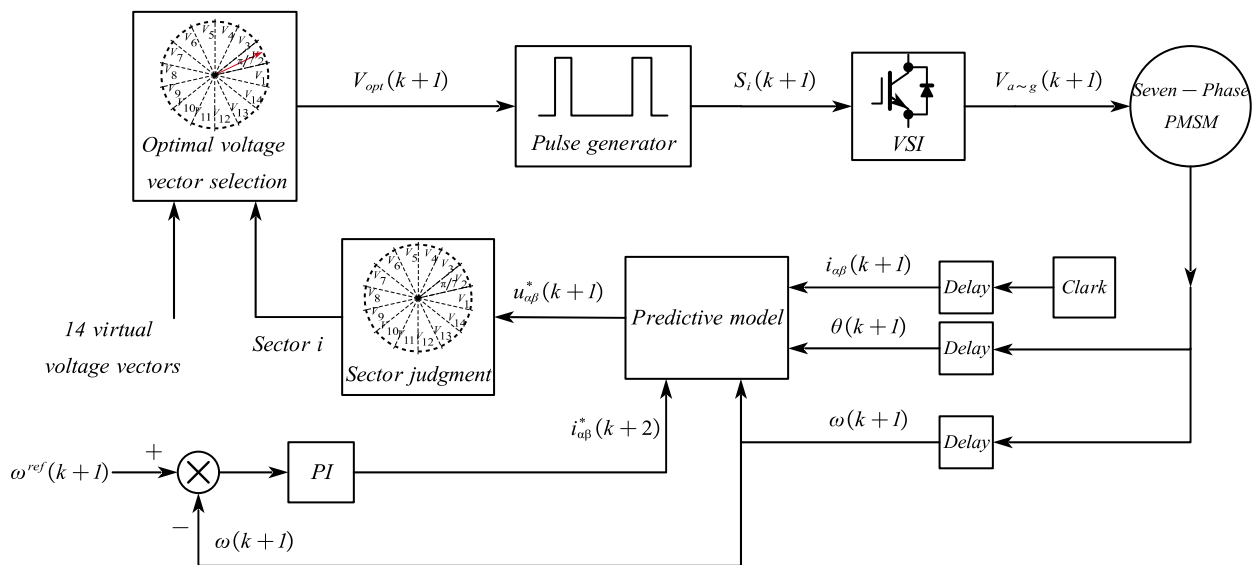


Fig. 3 Block diagram of costless function MPCC scheme.

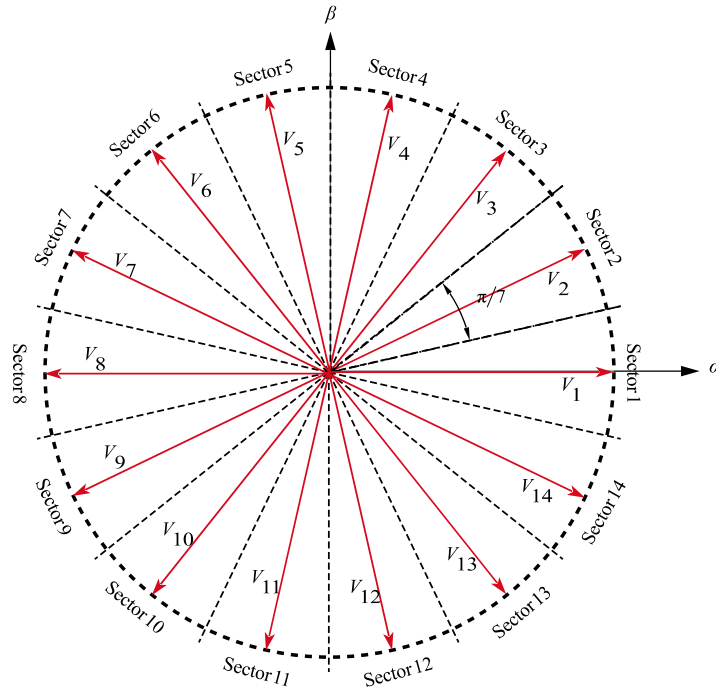


Fig. 4 Virtual space vector diagram in the  $\alpha\text{-}\beta$  plane.

Each virtual voltage vector is composed of 5 basic voltage vectors, take the virtual voltage vector  $V_2$  as an example, which is composed of voltage vectors 113, 97, 112, 99, 120, and its expression in  $\alpha\text{-}\beta$  space is as Eq. (12). The synthetic vector diagram in  $\alpha\text{-}\beta$ ,  $x_1\text{-}y_1$  and  $x_2\text{-}y_2$  space is shown in Fig. 5.

$$V_2 = t_1 \mathbf{99} + t_2 \mathbf{97} + t_3 \mathbf{113} + t_2 \mathbf{112} + t_1 \mathbf{120} \quad (12)$$

$$= t_1 (\mathbf{99} + \mathbf{120}) + t_2 (\mathbf{97} + \mathbf{112}) + t_3 \mathbf{113}$$

To suppress harmonics, the virtual voltage vector on the other spaces should be set to zero. Under this constraint, the time-factors  $t_1$ ,  $t_2$  and  $t_3$  can be calculated:

$$\begin{cases} t_1 (\mathbf{99}_{x_1 y_1} + \mathbf{120}_{x_1 y_1}) + t_2 (\mathbf{97}_{x_1 y_1} + \mathbf{112}_{x_1 y_1}) + t_3 \mathbf{113}_{x_1 y_1} = 0 \\ t_1 (\mathbf{99}_{x_2 y_2} + \mathbf{120}_{x_2 y_2}) + t_2 (\mathbf{97}_{x_2 y_2} + \mathbf{112}_{x_2 y_2}) + t_3 \mathbf{113}_{x_2 y_2} = 0 \\ 2t_1 + 2t_2 + t_3 = 1 \end{cases} \quad (13)$$

Form Eq. (13), the time-factors are:

$$\begin{cases} t_1 = 0.1980 \\ t_2 = 0.1588 \\ t_3 = 0.2862 \end{cases} \quad (14)$$

After substituting Eq. (14) into Eq. (12), the virtual voltage vector  $V_{2\alpha\beta} = 0.562V_{dc} \angle 25.71^\circ$  in  $\alpha\text{-}\beta$  space and zero on other spaces, is shown in Fig. 6.

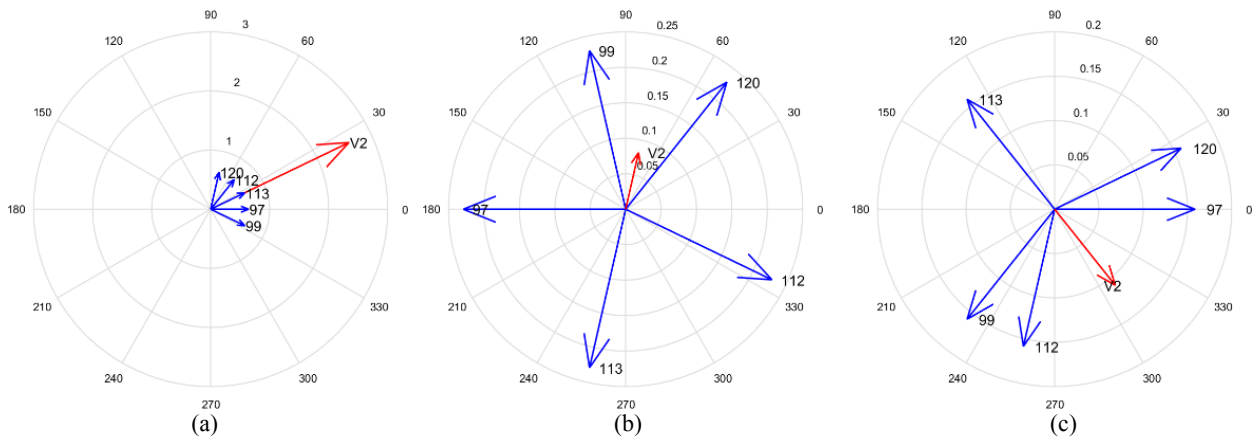
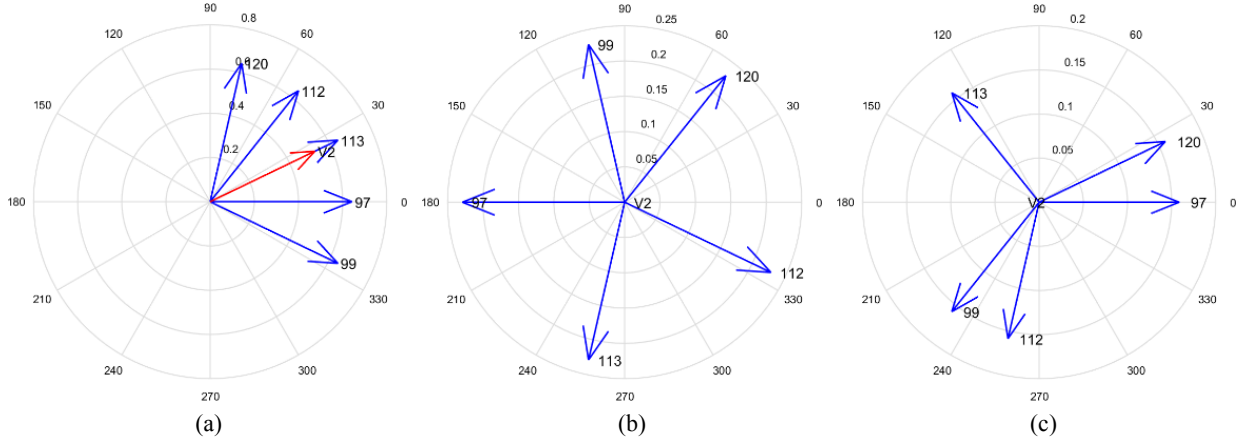


Fig. 5 Synthetic voltage vectors on different spaces: (a)  $\alpha\text{-}\beta$  subspace, (b)  $x_1\text{-}y_1$  subspace, (c)  $x_2\text{-}y_2$  subspace.



**Fig. 6** Optim voltage vectors  $V_2$  synthesized in different spaces under time-factor: (a)  $\alpha$ - $\beta$  subspace, (b)  $x_1$ - $y_1$  subspace, (c)  $x_2$ - $y_2$  subspace.

In a similar way, other virtual volume vectors can be synthesized. Fourteen (14) virtual voltage vectors will act as a finite control set for the MPCC, minimizing both the CMC and suppressing the 3rd and 5th harmonics at the same time.

#### 4.2 Switching Signal Generation

The optimal voltage vector in a sampling time  $T_s$  is one of the 14 virtual voltage vectors. By comparing the voltage vector calculated by the prediction model with the 14 virtual voltage vectors, the virtual voltage vector closest to the predicted voltage vector is selected as the optimal voltage vector at the current moment.

For example, when the predicted voltage vector is located in sector 2,  $V_2$  is selected as the optimal voltage vector at the same time, the action time voltage vectors 113, 97, 112, 99, 120 are expressed as:

$$\begin{cases} t_{99} = t_{120} = t_1 T_s \\ t_{97} = t_{112} = t_2 T_s \\ t_{113} = t_3 T_s \end{cases} \quad (15)$$

To effectively reduce the harmonics of SVPWM, a symmetrical pulse sequence is used to drive VSI. The half switching pulse of voltage vector  $V_2$  is shown in Fig. 7.  $S_i$  is the switch for each bridge arm.

### 5. System Simulation Results

The seven-phase PMSM module was built by SIMULINK module under MATLAB simulation tool

and the simulation real results were given in part 2.3 to verify the reasonableness of the model with the simulation parameters shown in Table 2.

The parameters of VSI: DC side voltage  $V_{dc} = 700$  V switching frequency  $f_c = 2.5 \times 10^4$  Hz, system sampling time  $T_s = 1 \times 10^{-4}$  s, and the output current frequency is 50 Hz.

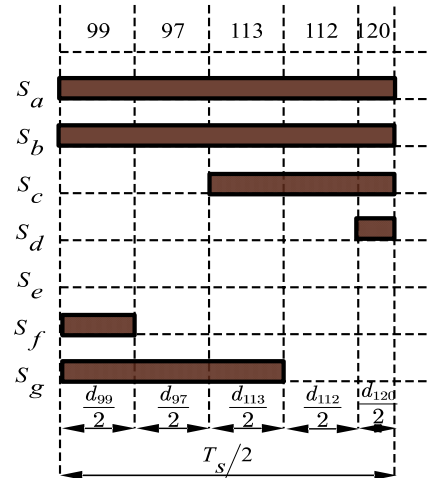


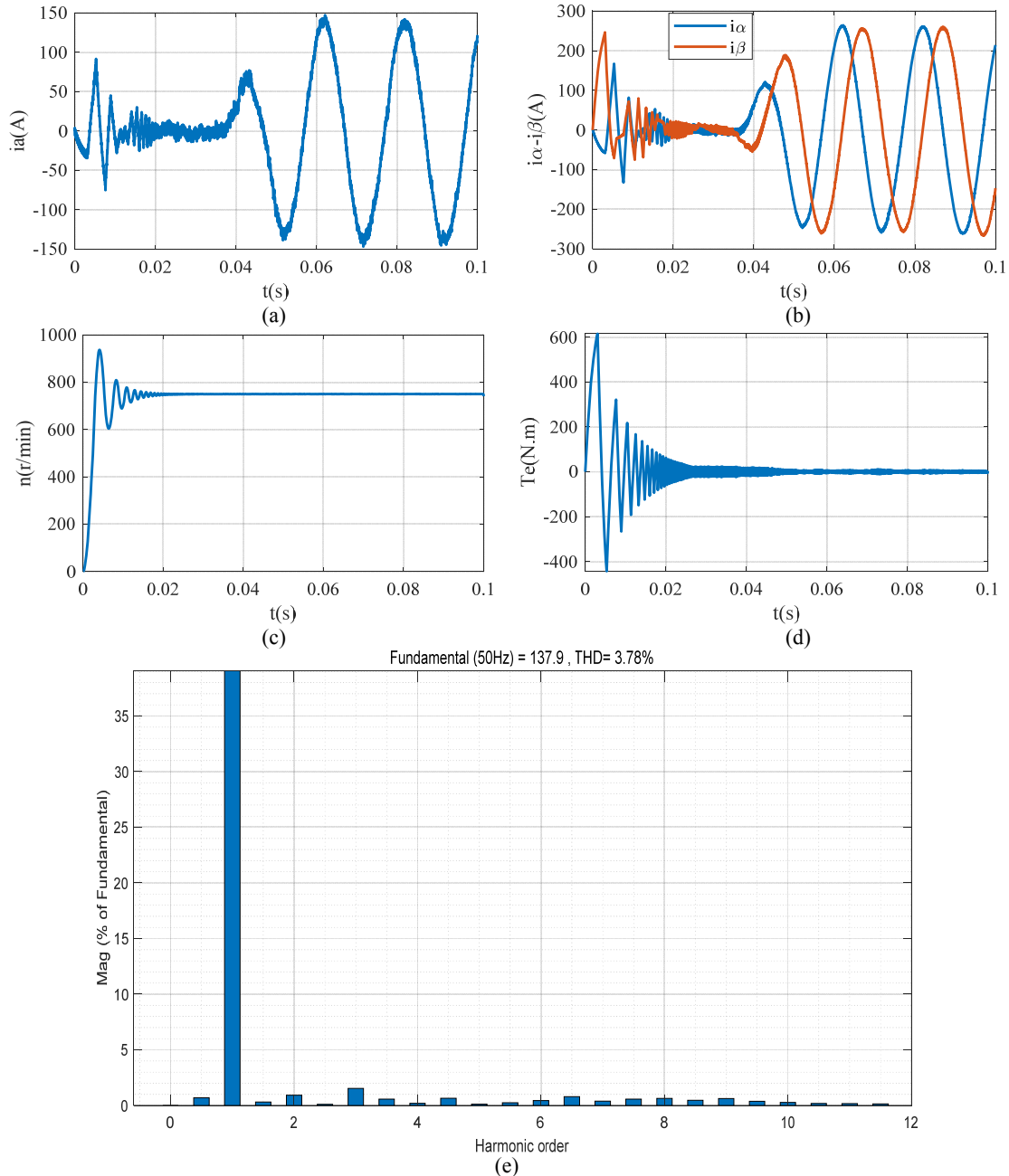
**Fig. 7** Half switching pulse of voltage vector  $V_2$ .

**Table 2** Motor parameters.

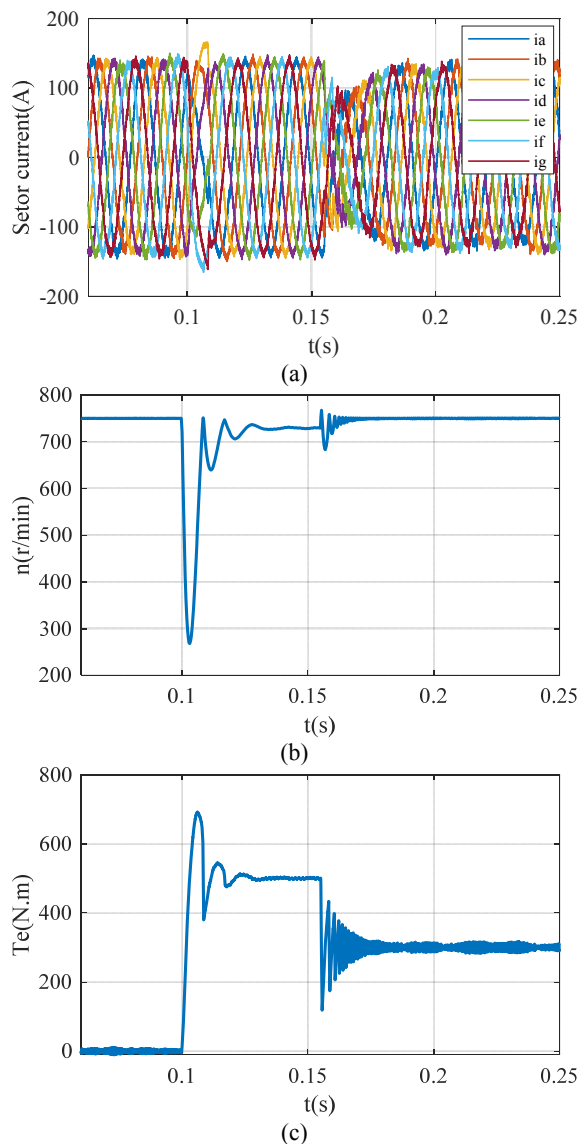
Parameters	Value
Number of phases	7
Stator leakage inductance $L_{ls}$	$3 \times 10^{-4}$ H
Stator mutual inductance $L_{ms}$	$1.2 \times 10^{-3}$ H
Stator resistance $R$	1.78 $\Omega$
Number of pole pairs $P_n$	4
Permanent magnet flux linkage $\psi$	0.175 Wb
Damping factor $B$	$0.4 \times 10^{-3}$
Moment of inertia $J$	0.015 kg·m <sup>2</sup>

Fig. 8 shows the stator current waveform after the motor reaches the steady state without load torture and the results of the FFT analysis of the stator current waveform. When the motor reaches steady state at no load, the motor stator current is a smooth sinusoidal function waveform, and after FFT analysis, the THD (Total Harmonic Distortion) accounts for only 3.78% of the fundamental component (50 Hz), of which the

3rd harmonic accounts for only 1.53% and the 5th harmonic accounts for only 0.12%. Rotor reaches a given speed of 750 r/min, a smooth rotation with no pulsation values. Maximum electromagnetic torque is 5 N·m. The simulation results show that the costless function MPCC strategy proposed in this paper effectively suppresses the harmonics generated by VSI and ensures the voltage quality of the system.



**Fig. 8 Simulation results in steady state: (a) phase A current waveform of stator, (b) current on  $\alpha$ - $\beta$  space, (c) rotor speed, (d) electromagnetic torque, (e) phase A current FFT analysis results.**



**Fig. 9 Dynamic response of motor under load: (a) stator phase current, (b) rotor speed, (c) electromagnetic torque.**

At the same time, the effect of the controller on the motor control under different load conditions is simulated. The simulation time is 0.25 s. At 0.1 s, the load torque increases to 500 N·m, and at 0.155 s, the load torque decreases to 300 N·m. In Fig. 9 the stator phase currents, rotor speed and electromagnetic torque are shown. After each phase current reaches steady state, the harmonic content is low; 0.025 s later the system reaches steady state and the speed and torque reach stable values. The speed fluctuates to some extent, but the fast dynamic response of the control system makes it very right and stable. When the

system is in steady state, the electromagnetic torque is equal to the load torque.

## 6. Conclusion

In this paper, the MPCC (model predictive current control) is applied to the current control of a two-level inverter, while the basic principle of MPCC of a seven-phase inverter is described with a seven-phase PMSM as the load, and the costless-function MPCC strategy is proposed to reduce the computation time and improve the dynamic performance of the system. The generation of the 3rd and 5th harmonics is suppressed under the optimal voltage vector based. In addition, the control system has only one speed PI regulator, which largely reduces the complexity of system commissioning compared to traditional dual PI regulators.

## References

- [1] Hasoun, M., Afia, A. E., Chikh, K., Khafallah, M., and Benkirane, K. 2018. "A PWM Strategy for Dual Three-Phase PMSM Using 12-Sector Vector Space Decomposition for Electric Ship Propulsion." In *Proceedings of 2018 19th IEEE Mediterranean Electrotechnical Conference (MELECON)*, 243-8. doi: 10.1109/MELCON.2018.8379101.
- [2] Xiong, C., Xu, H., Guan, T., and Zhou, P. 2020. "A Constant Switching Frequency Multiple-Vector-Based Model Predictive Current Control of Five-Phase PMSM with Nonsinusoidal Back EMF." *IEEE Trans. Ind. Electron.* 67 (3): 1695-707. doi: 10.1109/TIE.2019.2907502.
- [3] Dabour, S. M., Abdel-Khalik, A. S., Massoud, A. M., and Ahmed, S. 2019. "Analysis of Scalar PWM Approach with Optimal Common-Mode Voltage Reduction Technique for Five-Phase Inverters." *IEEE J. Emerg. Sel. Top. Power Electron.* 7 (3): 1854-71. doi: 10.1109/JESTPE.2018.2866028.
- [4] Pandit, J. K., Aware, M. V., Nemade, R. V., and Levi, E. 2017. "Direct Torque Control Scheme for a Six-Phase Induction Motor with Reduced Torque Ripple." *IEEE Trans. Power Electron.* 32 (9): 7118-29. doi: 10.1109/TPEL.2016.2624149.
- [5] Aberkane, H., Sakri, D., and Rahem, D. 2018. "Improvement of Direct Torque Control Performances Using FCS-MPC and SVM Applied to PMSM: Study and Comparison." In *Proceedings of 2018 International Conference on Electrical Sciences and Technologies in*

- Maghreb (CISTEM)*, 1-6. doi: 10.1109/CISTEM.2018.8613340.
- [6] Gashtil, H., Pickert, V., Atkinson, D., Giaouris, D., and Dahidah, M. 2019. "Comparative Evaluation of Field Oriented Control and Direct Torque Control Methodologies in Field Weakening Regions for Interior Permanent Magnet Machines." In *Proceedings of 2019 IEEE 13th International Conference on Compatibility, Power Electronics and Power Engineering (CPE-POWERENG)*, 1-6. doi: 10.1109/CPE.2019.8862320.
- [7] Hang, J., Zhang, J., Xia, M., Ding, S., and Hua, W. 2020. "Interturn Fault Diagnosis for Model-Predictive-Controlled-PMSM Based on Cost Function and Wavelet Transform." *IEEE Trans. Power Electron.* 35 (6): 6405-18. doi: 10.1109/TPEL.2019.2953269.
- [8] Wang, W., Fan, Y., Chen, S., and Zhang, Q. 2018. "Finite Control Set Model Predictive Current Control of a Five-Phase PMSM with Virtual Voltage Vectors and Adaptive Control Set." *CES Trans. Electr. Mach. Syst.* 2 (1): 136-41. doi: 10.23919/TEMS.2018.8326460.
- [9] Dang, Q., Guan, Z., Li, Q., Hu, R., and Hong, Z. 2019. "Advanced Model Predictive Control Strategy in Application of Permanent Magnet Synchronous Machine." In *Proceedings of 2019 14th IEEE Conference on Industrial Electronics and Applications (ICIEA)*, 1039-44. doi: 10.1109/ICIEA.2019.8834103.
- [10] Xin, L., and Bin, Z. 2018. "Sensorless Adaptive Sliding Mode FCS-MPC Using Extended State Observer for PMSM System." In *Proceedings of 2018 IEEE International Conference of Intelligent Robotic and Control Engineering (IRCE)*, 171-7. doi: 10.1109/IRCE.2018.8492967.
- [11] Rodriguez, J., and Cortes, P. 2012. *Predictive Control of Power Converters and Electrical Drives*. Accessed December 17, 2020. <https://ieeexplore.ieee.org/book/6198919>.
- [12] Walz, S., Lazar, R., and Liserre, M. 2018. "Multi-step Model Predictive Control for a High-Speed Medium-Power PMSM." In *Proceedings of 2018 IEEE Energy Conversion Congress and Exposition (ECCE)*, 5040-6. doi: 10.1109/ECCE.2018.8557732.
- [13] Ma, Z., Saeidi, S., and Kennel, R. 2014. "FPGA Implementation of Model Predictive Control with Constant Switching Frequency for PMSM Drives." *IEEE Trans. Ind. Inform.* 10 (4): 2055-63. doi: 10.1109/TII.2014.2344432.
- [14] Wang, Y., Wang, X. C., Xie, W., Wang, F. X., Dou, M. F., Kennel, R. M., Lorenz, R. D., and Gerling, D. 2017. "Deadbeat Model-Predictive Torque Control with Discrete Space-Vector Modulation for PMSM Drives." *IEEE Trans. Ind. Electron.* 64 (5): 3537-47. doi: 10.1109/TIE.2017.2652338.
- [15] Zhang, D., Xu, B., Yang, H., and Zhu, P. 2017. "Simulation Analysis of SVPWM Based on Seven-Phase Permanent Magnet Synchronous Motor." In *Proceedings of 2017 International Conference on Control, Automation and Information Sciences (ICCAIS)*, 251-6. doi: 10.1109/ICCAIS.2017.8217585.
- [16] Dordevic, O., Levi, E., and Jones, M. 2013. "A Vector Space Decomposition Based Space Vector PWM Algorithm for a Three-Level Seven-Phase Voltage Source Inverter." *IEEE Trans. Power Electron.* 28 (2): 637-49. doi: 10.1109/TPEL.2012.2203148.
- [17] Vu, H., and Lee, H. 2020. "Model Predictive Current Control Scheme for Seven-Phase Voltage Source Inverter with Reduced Common-Mode Voltage and Current Harmonics." *IEEE J. Emerg. Sel. Top. Power Electron.*, 1. doi: 10.1109/JESTPE.2020.3009392.